Titanium contacts to MoS_2 with interfacial oxide: Interface chemistry and thermal transport

Keren M. Freedy,[1,*] David H. Olson,[2,*] Patrick E. Hopkins,[1,2,3] and Stephen J. McDonnell[1]
[1]*Department of Materials Science and Engineering, University of Virginia, Charlottesville, Virginia 22904, USA*
[2]*Department of Mechanical and Aerospace Engineering, University of Virginia, Charlottesville, Virginia 22904, USA*
[3]*Department of Physics, University of Virginia, Charlottesville, Virginia 22904, USA*

(Received 17 March 2019; revised manuscript received 29 July 2019; published 4 October 2019)

The deposition of a thin oxide layer at metal/semiconductor interfaces has been previously reported as a means of reducing contact resistance in two-dimensional (2D) electronics. Using x-ray photoelectron spectroscopy with *in situ* Ti deposition, we fabricate $Au/Ti/TiO_x/MoS_2$ samples as well as $Au/Ti/MoS_2$ and $Au/TiO_x/MoS_2$ for comparison. Elemental titanium reacts strongly with MoS_2 whereas no interface reactions are observed in the two types of samples containing TiO_x/MoS_2 interfaces. Using time-domain thermoreflectance for measurements of thermal boundary conductance, we find that samples contacted with Ti and a thin TiO_x layer at the interface (∼1.5 nm) exhibit the same behavior as samples contacted solely with pure Ti. The $Au/TiO_x/MoS_2$ samples exhibit ∼20% lower thermal boundary conductance, despite having the same MoS_2 interface chemistry as the samples with thin oxide at the Ti/MoS_2 interface. We identify the mechanism for this phenomenon, attributing it to the different interfaces with the top Au contact. Our work demonstrates that the use of thin interfacial oxide layers to reduce electrical contact resistance does not compromise heat flow in 2D electronic devices. We note that the thicknesses of the Ti and TiO_x layers must be considered for optimal thermal transport.

DOI: 10.1103/PhysRevMaterials.3.104001

I. INTRODUCTION

Contact resistance presents a major obstacle to the success of two-dimensional (2D) electronics [1,2]. One approach to the reduction of electrical contact resistance is the deposition of thin oxide interlayers at the interface between the semiconductor and the metal [3–9]. Park *et al.* [3,4] have shown a reduction in electrical contact resistance and an improvement in device stability in MoS_2 field effect transistors with 2 nm TiO_2 films deposited by atomic layer deposition (ALD) at the interface between the MoS_2 and the Ti contact. The observed improvements were attributed to Fermi-level depinning and interface dipole effects. Kim *et al.* [5], who observed a decrease in Fermi-level pinning with 1 nm interfacial TiO_2, suggested that the presence of an interfacial oxide reduces the density of metal-induced gap states by blocking the penetration of the electron wave function from the metal. Similarly, Kaushik *et al.* [6] concluded from density functional theory that the Schottky barrier height is reduced due to charge-transfer doping from the TiO_2 layer to MoS_2. They have experimentally shown a 24-fold reduction in contact resistance and tenfold improvement in on-current and field-effect mobility.

While the use of an interfacial oxide has been found to be highly beneficial to electronic properties in the aforementioned studies, thermal characterization of this interface is relatively lacking. An understanding of thermal transport is crucial as thermal resistances at the contact interface can inhibit heat removal from 2D electronic devices, compromising their performance and reliability [10]. The thermal conductance at the MoS_2/SiO_2 substrate interface present in most 2D devices is typically low, $\sim 14\,\mathrm{MW\,m^{-2}\,K^{-1}}$ [11]. Therefore caution must be taken when introducing additional interfaces to the device that could potentially increase the total resistance of the system. Our previous work has shown that transport across contact interfaces is highly sensitive to the oxide composition of Ti for graphene as well as bulk substrates [12,13]. McDonnell *et al.* [14] have demonstrated that Ti/MoS_2 and TiO_2/MoS_2 interfaces exhibit vastly different chemical compositions and suggested potential detrimental effects on thermal transport due to the higher thermal resistance of TiO_2 compared to metallic Ti. They noted that work by Duda *et al.* [15] concludes that the removal of native oxide along with the deposition of a Ti adhesion layer has been found to be critical to lowering thermal resistances at metal-semiconductor interfaces. Similarly, Hopkins *et al.* [16] have shown a substantial decrease in thermal boundary conductance due to the presence of native oxides at metal-semiconductor interfaces. Density functional theory calculations conclude that phonon-phonon coupling and phonon transmission across the metal/MoS_2 interface is strongly dependent on the degree of orbital hybridization at the contact, and that stronger chemical and electronic interactions at the contact result in higher thermal boundary conductance [17,18]. This would imply that the inclusion of oxide instead of metal at the MoS_2 interface could potentially result in diminished thermal transport, warranting an investigation of the thermal boundary conductance across Ti contacts to MoS_2 with interfacial oxides, and the potential dependence of thermal boundary conductance on interface chemistry.

*These authors contributed equally to this work.

 ©2019 American Physical Society

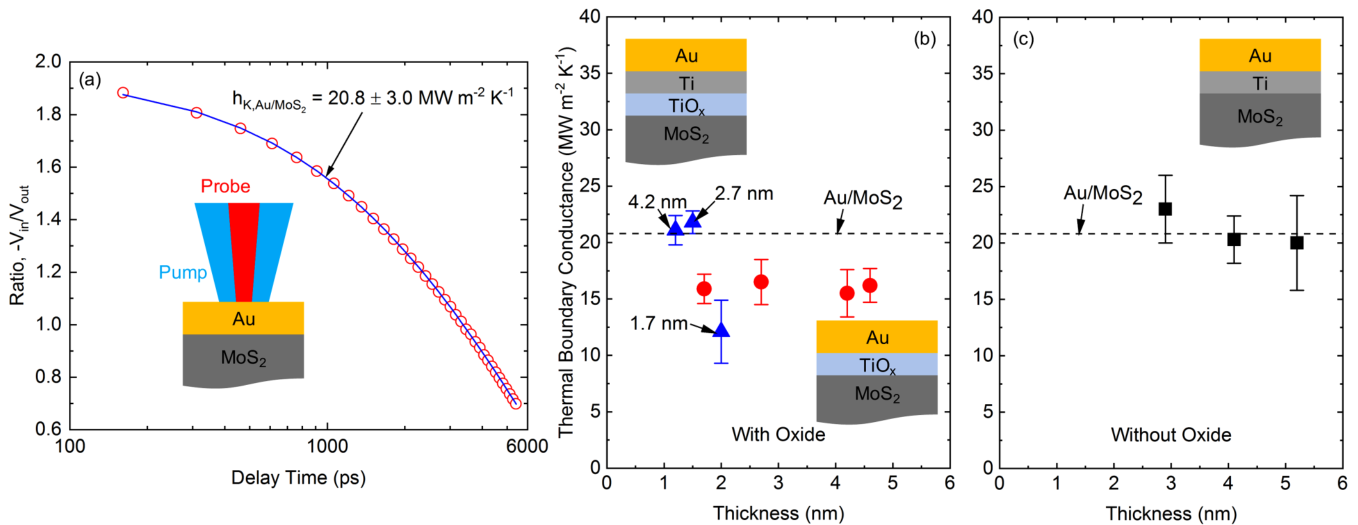

FIG. 1. (a) TDTR data and best fit for the Au/MoS_2 structure. Thermal boundary conductance as a function of interfacial layer thickness for the MoS_2 substrates (b) with and (c) without an oxide interlayer. Samples included are Au/Ti (black squares), Au/TiO_x (red circles), and Au/Ti/TiO_x (blue triangles) in addition to a reference sample of Au/MoS_2 (dashed line). The arrows indicate the Ti metal thickness for each Ti/TiO_x sample where data are plotted as a function of oxide thickness.

II. EXPERIMENTAL METHODS

We report a process for electron-beam deposition of an interfacial Ti oxide layer in ultrahigh vacuum (UHV) using a partial pressure of O_2. The process allows for *in situ* chemical characterization of the interface with x-ray photoelectron spectroscopy (XPS). We compare the effects of metal (Ti), oxide (TiO_x), and metal/oxide heterostructure (Ti/TiO_x) films, at a range of thicknesses, deposited on bulk geological MoS_2 crystals that are typically used for device fabrication. We use time-domain thermoreflectance (TDTR), an optical pump probe technique, for the measurement of thermal boundary conductance across these interfaces [19–21]. By measuring bulk geological crystals we are able to bypass thermal resistances from substrate/MoS_2 interfaces and solely characterize the contact interfaces associated with the MoS_2 surface.

Prior to loading to UHV, bulk MoS_2 geological crystals (purchased from SPI [22]) were exfoliated with Scotch tape to clean the surface by removing the top layer [14]. Preliminary XPS data were collected in our Scienta Omicron UHV system [23]. All XPS data were acquired at a pass energy of 50 eV, using an Al $K\alpha$ source with a photon energy of 1486.7 eV. The Mantis QUAD-EVC 4 pocket evaporator was used to deposit Ti onto the sample *in situ*. The titanium was evaporated at a rate of approximately 1 Å/min. For oxide deposition, a pressure of 5×10^{-6} mbar of ultrahigh-purity O_2 was maintained in the chamber during deposition. XPS data were acquired after each Ti and TiO_x deposition. See the Supplemental Material [24] (Sec. S5) for the calculation procedure for the thickness of the deposited layers using the attenuation of the Mo 3*d* core-level intensity. The samples were then capped with 1–2 nm Au *in situ* to prevent oxidation in air upon removal from UHV. An additional ~70 nm of Au was deposited in an *ex situ* *e*-beam evaporator for TDTR measurements.

TDTR is an optical pump probe technique that is widely used to characterize interfacial conductance at a variety of metal contacts. An 80 MHz repetition rate laser centered at 800 nm is split into high-power pump and low-power probe paths. The pump is amplitude modulated using an electro-optic modulator, and frequency doubled to 400 nm before being focused on the sample surface. The probe is mechanically delayed in time, and monitors the thermoreflectance at the sample surface due to temperature perturbations induced by the pump. We specifically modulate the pump at 10.28 MHz to ensure one-dimensionality in our analysis and minimize sensitivity to potential in-plane transport in the MoS_2. Indeed, MoS_2 in its few-layer and bulk forms has been shown experimentally to have an anisotropic thermal conductivity [25–28]. Modulating at this frequency also improves our sensitivity to the interfacial conductance at these contacts. We estimate the temperature rise of the MoS_2 to be on the order of ~30 K due to the average absorbed power from the pump and probe beams during TDTR experiments, which we calculate based on in- and cross-plane thermal conductivities of MoS_2 from the literature [21,25,26] and the numerical solution to the multilayer cylindrically symmetric heat equation used to analyze our TDTR data. Example TDTR data and best fit are shown in Fig. 1(a) for the Au/MoS_2 specimen, where we extract a conductance of $20.8 \pm 3.0\,\mathrm{W\,m^{-2}\,K^{-1}}$. The error in our reported values reflect the standard deviation from several measurements on each specimen, as well the uncertainty associated with an 8% deviation in the thickness of the Au capping layer. More information regarding TDTR and its analyses can be found in the literature [19,21]. See the Supplemental Material [24] (Sec. S1) for a description of our two-color implementation of TDTR as well as a sensitivity analysis of relevant parameters in the Au/MoS_2 system.

III. RESULTS AND DISCUSSIONS

Thermal boundary conductance, h_K, is plotted for structures with and without TiO_x in Figs. 1(b) and 1(c),

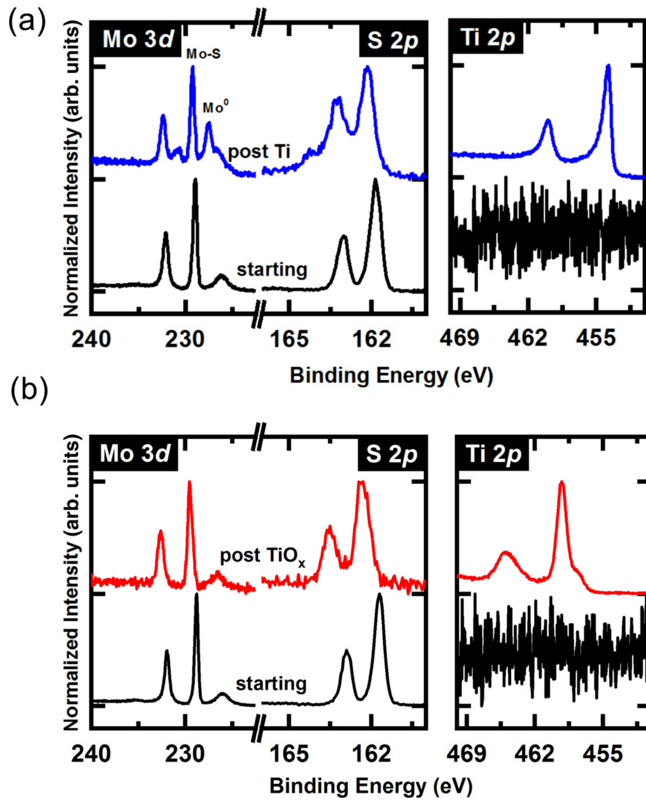

FIG. 2. Core-level XPS spectra before and after the deposition of (a) 4.1 nm Ti on MoS_2 and (b) 4.6 nm TiO_x on MoS_2.

respectively. In the limit of zero TiO_x thickness, corresponding to samples with pure Ti metal overlayers ($Au/Ti/MoS_2$), the average h_K value was approximately $21.5 \pm 5.6\,MW\,m^2\,K^{-1}$. This value is roughly equivalent to the h_K value of the Au/MoS_2 reference sample ($20.8 \pm 3.0\,MW\,m^2\,K^{-1}$). The results are also consistent with previously measured values of metal/MoS_2 interfaces [25,29]. We note that the three $Au/Ti/MoS_2$ samples had Ti thicknesses ranging from 2.9 to 5.2 nm and Ti metal thickness had no effect on h_K for these samples, suggesting that the intrinsic resistance of the Ti does not contribute to the overall resistance of the system. Similarly, the figure shows that TiO_x/MoS_2 samples with TiO_x thicknesses from 1.7 to 4.6 nm all exhibit roughly the same value of $16.0 \pm 2.8\,MW\,m^2\,K^{-1}$. The lack of thickness dependence of h_K in the Ti/MoS_2 and TiO_x/MoS_2 samples indicates that thermal transport is dominated by interfacial resistances and not by the intrinsic thermal resistance of metal or oxide layers.

Chemical characterization of the Ti/MoS_2 and TiO_x/MoS_2 interfaces is shown in Fig. 2. We implement XPS so as to observe any chemical changes in the underlying MoS_2 when in contact with Ti or TiO_x. See the Supplemental Material [24] (Sec. S3) for the core-level spectra of all specimens examined in this study. Figure 2(a) shows the core-level XPS spectra before and after the deposition of 4.1 nm Ti metal in UHV. Before the deposition of Ti metal (black curve), MoS_2 is characterized by the Mo $3d_{5/2}$ state at $\sim$228.9 eV with a spin-orbit splitting value of 3.1 eV, and the S $2p_{3/2}$ state at $\sim$161.8 eV with a spin-orbit splitting of 1.2 eV. Following the deposition of Ti, the spectra exhibit new chemical states including Mo metal (Mo^0) at 227.5 eV in the Mo 3*d* spectrum and Ti-S states in the S 2*p* spectrum. This result is consistent with previous reports of the deposition of Ti in UHV [14].

Figure 2(b) shows XPS spectra corresponding to a sample with 4.6 nm of TiO_x. The spectra indicate that the Mo-S bonds are preserved and no chemical reaction occurs between Ti and the substrate. As previously reported by McDonnell *et al.* [14], the presence of a partial pressure of oxygen during the deposition of Ti on MoS_2 inhibits the reaction between them as Ti reacts with oxygen impinging on the surface of the substrate during deposition. The Mo 3*d* and S 2*p* core levels exhibit a 0.64 eV shift to higher binding energy, corresponding to a change in the position of the Fermi level. This indicates that the presence of an oxide overlayer causes *n*-type doping in the sample. This result is similar to that of Kaushik *et al.* [6] who reported a 0.5 eV core-level shift for 2 nm of ALD TiO_2 on MoS_2. We note that the oxide which forms under the deposition conditions in our UHV chamber comprises two chemical states. The TiO_2 state has its $2p_{3/2}$ component at 459.2 eV with a spin-orbit splitting of 5.7 eV and comprises $\sim$80% of the oxide layer deposited. The second chemical state, which appears at 457.65 eV with a spin-orbit splitting of 5.5 eV corresponds to Ti_2O_3 [30,31]. See the Supplemental Material [24] (Sec. S4) for the spectral deconvolution of the oxide layer.

Unlike the pure metal and oxide samples, h_K of the $Au/Ti/TiO_x/MoS_2$ samples exhibits a decrease with increasing oxide thickness, with no apparent dependence on metallic Ti thickness, as shown in Fig. 1. The two samples with TiO_x thicknesses $\leqslant$1.5 nm have h_K values comparable to that of the $Au/Ti/MoS_2$ and Au/MoS_2 samples, whereas the $Au/Ti(1.7\,nm)/TiO_x(2.0\,nm)/MoS_2$ is comparable to the $Au/TiO_x/MoS_2$ samples with no metal overlayer, within uncertainty. The reduction in h_K for this sample could be due to two possible reasons. The first is the increase in the oxide thickness compared to the heterostructures with TiO_x thickness $\leqslant$1.5 nm. However, given that no oxide thickness dependence for h_K of the $Au/TiO_x/MoS_2$ samples is observed, the increased oxide thickness is unlikely to be the dominant factor here. The second explanation is that the thickness of the Ti in the heterostructure (1.7 nm) is quite thin. From previous works, it has been shown that a reduction in the interfacial conductance is observed as the thickness of an interfacial adhesion layer becomes very thin (e.g., Cu and Cr) [32]. This reduction in our experiment is explained using similar predictions of accumulated thermal boundary conductance, whereby phonons in Ti with wavelengths less than the total Ti thickness participate in transport across the interface. In this way, the reduction in the population of Ti phonons due to a decrease in total Ti thickness ultimately results in a reduced h_K at the interface. We believe this to be the case when the thickness of the Ti becomes very thin in the heterostructures, making our results consistent with those of Jeong *et al.* [32].

The XPS spectra of a $Ti(2.7\,nm)/TiO_x(1.5\,nm)/MoS_2$ sample are shown in Fig. 3. The TiO_x/MoS_2 interface (red curve) is chemically identical to that shown in Fig. 2(b), exhibiting a *n*-type Fermi-level shift and no other chemical changes following the deposition of Ti metal (blue curve). The only observable changes are broadening of the peaks

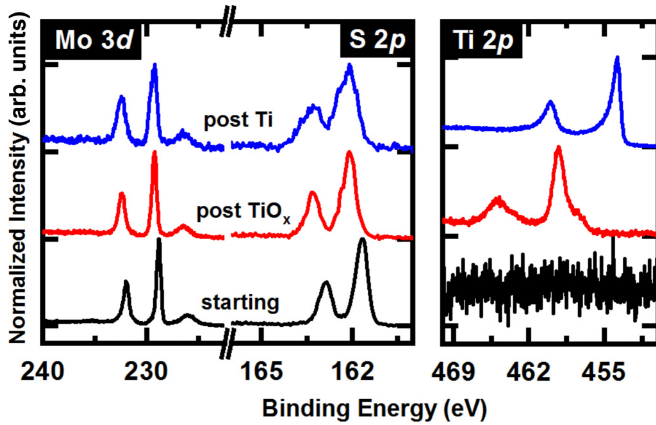

FIG. 3. Core-level XPS spectra of the Ti/TiO_x/MoS_2 samples.

and an increase in noise, which occurs due to scattering and attenuation in the TiO_x and Ti overlayers [33]. The lack of interface reactions with the presence of interfacial oxide is one possible explanation for the Fermi-level depinning effect reported by others [3–5]. Fermi-level pinning has been attributed to interfacial reaction products which create new electronic states within the semiconductor band gap [34]. By blocking interface reactions via direct contact with an unreactive oxide layer, MoS_2 retains its intrinsic band structure with no new states which could pin the Fermi level.

It is clear from comparison of Figs. 2(b) and 3 that interface chemistry does not explain the differences in behavior of h_K, as the TiO_x/MoS_2 interfaces in both the pure oxide and metal/oxide samples are chemically identical. Therefore, the behavior of h_K is likely dominated by one of the other interfaces present in the device. For the metal/oxide heterostructure, these interfaces include Au/Ti and Ti/TiO_x, whereas the oxide sample contains only Au/TiO_x. The resistance from the Au/Ti interface is not a contributing factor, since thermal transport across metal/metal interfaces is governed by electrons near the Fermi energy, yielding thermal boundary conductance values that are far higher than those across metal/nonmetal interfaces (i.e., negligible thermal resistances at these metal/metal interfaces) [35–38]. The negligible contribution of this interface is evident in Fig. 1, which shows that Au/Ti/MoS_2 exhibits the same h_K as the Au/MoS_2 reference sample, and is consistent with previous measurements of thermal boundary conductance at Au/graphene and Au/Ti/graphene interfaces [39].

To determine the extent of the contribution of the thermal conductances across the Au/TiO_x, Au/Ti, and Ti/TiO_x interfaces to the overall measured h_K, we fabricated several reference samples. The samples included Au/Ti (2.3 nm)/Au/O/Au, Au/TiO_x (2.0 nm)/Au/O/Au, and Au/Ti(2.2 nm)/TiO_x(4.4 nm)Au/O/Au. The appearance of O at the interface arises due to residual oxygen present at the Au/Au interface following a UV-O_3 treatment, as discussed later. By measuring h_K from each of these stacks we are able to isolate each of the interfaces and determine the interface contributions to the measured h_K from series resistance model. See Supplemental Material [24] (Sec. S2) for further discussion of the specific model implemented. We first deposited 80 nm Au on single-crystal sapphire (Al_2O_3) with a 5 nm Al adhesion layer in a cleanroom evaporator at high vacuum (HV). Al_2O_3 was selected as our substrate to maximize sensitivity to potentially large conductances. The conductance at the Au/Al/Al_2O_3 interface was found to be $49 \pm 5.0\,\mathrm{MW\,m^{-2}\,K^{-1}}$. Following this measurement, the surface of the Au was cleaned via UV-O_3 exposure as described elsewhere [40] to remove adventitious carbon. The sample was loaded back into UHV. Since the process was found to leave residual oxygen on the Au surface, the sample was capped with ~2 nm Au in UHV to create a pristine surface before depositing subsequent Ti layers. Three separate samples with Ti (2.3 nm), TiO_x (2 nm), and Ti(2.2 nm)/TiO_x(4.4 nm) were created and capped with ~1-2 nm Au. To account for the contribution of residual oxygen at the interface between the HV and UHV Au, we fabricate a reference sample that is a UV-O_3 treated HV Au sample that is then capped with Au in UHV. This sample is measured to determine the contribution of the oxygenated Au interface to the total interfacial conductance in structures containing Ti and TiO_x.

Following the UHV deposition processes, the samples were transferred back to the HV electron-beam evaporator, and capped with ~67 nm of Au following an O_2 plasma cleaning procedure. TDTR was performed on the samples, fitting for the conductance across the newly deposited interfacial structure as the underlying Au/Al/Al_2O_3 interfacial conductance was measured prior to the deposition of the structures. The conductance across the Au/Au interface containing residual oxygen from the UV-O_3 process is measured to be $376 \pm 31\,\mathrm{MW\,m^{-2}\,K^{-1}}$, and is accounted for in subsequent derivations of Au/Ti and Au/TiO_x conductances. When accounting for this additional resistance, h_K of the Au/Ti interface is found to be $1680 \pm 190\,\mathrm{MW\,m^{-2}\,K^{-1}}$. We estimate this to be the lower bound for the conductance at the Au/Ti interface, based on the limitations of TDTR to measure ultrahigh boundary conductances, quasiballistic influences as a result of the thinness of the Ti layer, and extrinsic or chemical effects that prevent the Au/Ti interface from being an otherwise perfect interface. An additional possible explanation will be addressed later. Regardless, the conductance of metal-metal interfaces is quite high—the electron diffuse-mismatch model predicts a conductance of $5970\,\mathrm{MW\,m^{-2}\,K^{-1}}$ at the Au/Ti interface at room temperature [35]. Thus, the contribution of the Au/Ti interface in the total interfacial resistance is negligible compared to other resistances present in these systems.

The Au/TiO_x (2 nm)/Au/O/Au conductance is measured to be $44.5 \pm 3.2\,\mathrm{MW\,m^{-2}\,K^{-1}}$, resulting in an interfacial conductance at the Au/TiO_x interface to be $101 \pm 11\,\mathrm{MW\,m^{-2}\,K^{-1}}$, once the Au/O/Au interface is accounted for. The measured conductance across the Au/Ti(2.2 nm)/TiO_x(4.4 nm)/Au interface is $65.2 \pm 4.5\,\mathrm{MW\,m^{-2}\,K^{-1}}$, and suggests that the conductance of the Ti/TiO_x interface, with a value of $459 \pm 87\,\mathrm{MW\,m^{-2}\,K^{-1}}$, is large compared to that across the Au/TiO_x. Our results imply that the Au/TiO_x interface presents a non-negligible thermal resistance due to the relative weak atomic interactions between Au and TiO_x; in fact, in the case of this Au/TiO_x/Au/Al/Al_2O_3 multilayer film system, the Au/TiO_x offers the limiting thermal resistance to heat flow. See the Supplemental Material [24] (Sec. S2) for a complete derivation of the above values.

TABLE I. Measured and derived values of Ti/TiO_x structures on MoS_2 and sandwiched between Au.

Interface	Au/Ti[a]	Au/TiO_x[a]	Ti/TiO_x[a]	Au/MoS_2	$Au/Ti/MoS_2$	$Au/TiO_x/MoS_2$	$Au/Ti/TiO_x/MoS_2$[b]	TiO_x/MoS_2[a]
$h_K (MW\,m^{-2}\,K^{-1})$	1680 ± 190	101 ± 11	459 ± 87	20.8 ± 1.1	21.1 ± 5.7	16.0 ± 2.8	21.5 ± 1.6	19.1 ± 3.8
$R_K (m^2\,K\,GW^{-1})$	0.59 ± 0.07	9.91 ± 1.07	2.18 ± 0.41	48.1 ± 2.54	47.4 ± 12.8	62.5 ± 10.9	46.5 ± 3.46	52.4 ± 10.4

[a]Denotes values that are derived from measurements.
[b]Denotes the average of the heterostructures with TiO_x thicknesses of 1.5 and 2.0 nm, omitting that with 1.7 nm Ti. Other values are averaged from all samples of that type.

The thermal conductance across the $Au/TiO_x/MoS_2$ interface can be modeled with a series resistance approach:

$$\frac{1}{h_{K,meas}} = \frac{1}{h_{K,Au/TiO_x}} + \frac{1}{h_{K,TiO_x/MoS_2}},$$

where $h_{K,meas}$ is the measured conductance across the $Au/TiO_x/MoS_2$ interface (averaged over all TiO_x thicknesses), $1/h_{K,Au/TiO_x}$ is the resistance of the Au/TiO_x interface, and $1/h_{K,TiO_x/MoS_2}$ is the resistance of the TiO_x/MoS_2 interface. Again, we neglect the contribution from the intrinsic resistance of the TiO_x layer based on the constant boundary conductance observed for the range of TiO_x thicknesses that are presented in Fig. 1. Taking $h_{K,meas}$ to be $16.0 \pm 2.8\,MW\,m^{-2}\,K^{-1}$, and $h_{K,Au/TiO_x}$ from our measurements on this control interface discussed above, we calculate $h_{K,TiO_x/MoS_2}$ to be $19.1 \pm 3.8\,MW\,m^{-2}\,K^{-1}$. The larger comparable conductance at the TiO_x/MoS_2 interface as compared to $h_{K,meas}$ suggests that the Au/TiO_x interfacial conductance is again playing a non-negligible role in the reduction of heat transport across these interfaces, albeit the TiO_x/MoS_2 represents the dominant thermal resistance in this system. This reduction can be circumvented by implementing a Ti/TiO_x heterostructure at the interface, provided that the Ti layer is thicker than ∼2 nm as discussed previously, whereby we see an increased boundary conductance as compared to just a TiO_x adhesion layer. In all, this also suggests that the Ti/TiO_x conductance is negligible compared to that of the Au/TiO_x and TiO_x/MoS_2 interface, allowing for a compromise of transport properties from both an electrical and thermal perspective. The values of the various interfaces with Ti and MoS_2 are summarized in Table I.

XPS characterization of the Au/Ti and Au/TiO_x interfaces shows that chemical bonding occurs at Au/Ti interfaces while no chemical interactions are observed in Au/TiO_x interfaces. The formation of intermetallic compounds in Au/Ti interfaces deposited in UHV at room temperature has been reported previously [41–43]. Figure 4 shows XPS acquired on Ti and TiO_x samples deposited in our UHV system before and after the deposition of ∼3 Å of Au. In the Ti $2p$ spectrum of the Ti metal sample shown in (a), the spectrum exhibits a core-level shift of 0.15 eV as well as broadening due to the presence of Au-Ti bonding at the interface following the deposition of Au. The TiO_x spectra shown in (b) acquired before and after Au deposition overlap perfectly showing no change in binding energy or line shape. In the Au $4f$ spectrum in (c), Au deposited on Ti exhibits a prominent asymmetry and a 0.33 eV shift to higher binding energy which is characteristic of intermetallic formation [44], while Au deposited on TiO_x retains the line shape and binding energy of elemental Au indicating no interaction occurs. The observed bonding at the Au/Ti interface is a potential explanation for the lower measured h_K of the Au/Ti interface in comparison with the value calculated based on the electron diffuse-mismatch model, which does not account for the formation of an intermetallic compound at the interface [35]. It has been shown previously that the thermal boundary conductance can become dominated by the

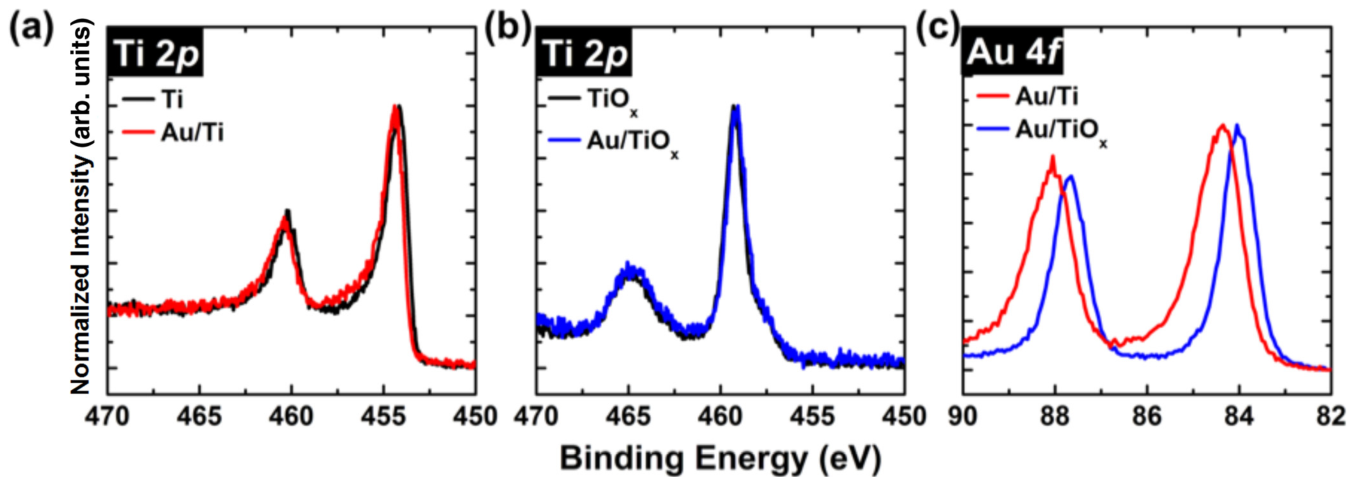

FIG. 4. Ti $2p$ spectra acquired on (a) Ti and (b) TiO_x films before and after the deposition of Au, with Au $4f$ spectra corresponding to these samples shown in (c).

thermal conductance of an interfacial compound layer [35]. Furthermore, intermetallic compounds have been found to exhibit low values of thermal conductivity in comparison with their pure metal constituents [45]. Nevertheless, the electron mediated thermal transport at the metallic Au/Ti interface results in a h_K value that is far higher than that corresponding to Au/TiO_x.

We note that while the conductance of the $Au/Ti/MoS_2$ interface is similar to that of the $Au/Ti/TiO_x/MoS_2$ interface, and offers improved thermal management as compared to using TiO_x alone, the use of Ti inherently modifies the underlying MoS_2. In devices contingent on just a monolayer of the dichalcogenide, where the electronic density of states departs significantly from its bulk counterpart [46,47], metallization, even in the absence of bond scission, has been shown to significantly impact the localized density of states [47,48]. Contrarily, after depositing TiO_x, we do not see the appearance of the Mo^0 state, suggesting a lack of stoichiometric redistribution. TiO_2 in contact with MoS_2 has also been previously shown to not heavily alter the density of states in each material, as they still maintain direct band gaps [49]. This, combined with the improved conductance when implementing a Ti/TiO_x heterostructure as an adhesion layer, offers a unique avenue for managing thermal and electronic transport properties in material systems contingent on the integration of MoS_2.

IV. CONCLUSIONS

In summary, we find that $Au/TiO_x/MoS_2$ exhibits ~20% lower thermal boundary conductance than $Au/Ti/MoS_2$. Samples with a thin TiO_x layer (~1–1.5 nm) at the interface between Ti and MoS_2 exhibit the same thermal boundary conductance as those with pure Ti metal. The difference in h_K between the TiO_x/MoS_2 and $Ti/TiO_x/MoS_2$ samples is observed despite the chemically identical TiO_x/MoS_2 interfaces present in both samples. The differences in h_K arise due to the different interfaces with the top Au contact. Whereas Au/Ti has negligible resistance, that of Au/TiO_x is substantial making this interface the dominant resistor in the system. Our results suggest that thin interfacial oxide layers which can be used to enhance electronic properties have no negative impact on thermal transport in 2D electronic devices. The thickness of the Ti layer in the Ti/TiO_x structure must be considered when implementing this type of contact.

ACKNOWLEDGMENTS

We appreciate funding from the US Department of Defense, Multidisciplinary University Research Initiative through the Army Research Office, Grant No. W911NF-16-1-0406. D.H.O. is grateful for funding from the National Defense Science and Engineering (NDSEG) and Virginia Space Grant Consortium (VSGC) fellowships.

[1] A. Allain, J. Kang, K. Banerjee, and A. Kis, Nat. Mater. **14**, 1195 (2015).

[2] H. Liu, A. T. Neal, and P. D. Ye, ACS Nano **6**, 8563 (2012).

[3] W. Park, Y. Kim, L. Sang Kyung, U. Jung, Y. Jin Ho, C. Cho, K. Yun Ji, L. Sung Kwan, H. In Seol, H. Lee, and L. Byoung Hun, in *Proceedings of the 2014 IEEE International Electron Devices Meeting* (San Francisco, CA, 2014), p. 5.1.1.

[4] W. Park, J. W. Min, S. F. Shaikh, and M. M. Hussain, Phys. Status Solidi A **214**, 1700534 (2017).

[5] G.-S. Kim, S.-H. Kim, J. Park, K. H. Han, J. Kim, and H.-Y. Yu, ACS Nano **12**, 6292 (2018).

[6] N. Kaushik, D. Karmakar, A. Nipane, S. Karande, and S. Lodha, ACS Appl. Mater. Interfaces **8**, 256 (2016).

[7] A. Agrawal, J. Lin, M. Barth, R. White, B. Zheng, S. Chopra, S. Gupta, K. Wang, J. Gelatos, S. E. Mohney, and S. Datta, Appl. Phys. Lett. **104**, 112101 (2014).

[8] J.-R. Chen, P. M. Odenthal, A. G. Swartz, G. C. Floyd, H. Wen, K. Y. Luo, and R. K. Kawakami, Nano Lett. **13**, 3106 (2013).

[9] A. Dankert, L. Langouche, M. V. Kamalakar, and S. P. Dash, ACS Nano **8**, 476 (2014).

[10] E. Pop, Nano Res. **3**, 147 (2010).

[11] E. Yalon, C. J. McClellan, K. K. H. Smithe, M. Muñoz Rojo, R. L. Xu, S. V. Suryavanshi, A. J. Gabourie, C. M. Neumann, F. Xiong, A. B. Farimani, and E. Pop, Nano Lett. **17**, 3429 (2017).

[12] K. M. Freedy, A. Giri, B. M. Foley, M. R. Barone, P. E. Hopkins, and S. McDonnell, Nanotechnology **29**, 145201 (2018).

[13] D. H. Olson, K. M. Freedy, S. J. McDonnell, and P. E. Hopkins, Appl. Phys. Lett. **112**, 171602 (2018).

[14] S. McDonnell, C. Smyth, C. L. Hinkle, and R. M. Wallace, ACS Appl. Mater. Interfaces **8**, 8289 (2016).

[15] J. C. Duda, C. Y. P. Yang, B. M. Foley, R. Cheaito, D. L. Medlin, R. E. Jones, and P. E. Hopkins, Appl. Phys. Lett. **102**, 081902 (2013).

[16] P. E. Hopkins, L. M. Phinney, J. R. Serrano, and T. E. Beechem, Phys. Rev. B **82**, 085307 (2010).

[17] Z. Yan, L. Chen, M. Yoon, and S. Kumar, ACS Appl. Mater. Interfaces **8**, 33299 (2016).

[18] R. Mao, B. D. Kong, and K. W. Kim, J. Appl. Phys. **116**, 034302 (2014).

[19] A. J. Schmidt, X. Chen, and G. Chen, Rev. Sci. Instrum. **79**, 114902 (2008).

[20] P. E. Hopkins, J. R. Serrano, L. M. Phinney, S. P. Kearney, T. W. Grasser, and C. T. Harris, J. Heat Transfer **132**, 081302 (2010).

[21] D. G. Cahill, Rev. Sci. Instrum. **75**, 5119 (2004).

[22] J.-M. Martin, C. Donnet, T. Le Mogne, and T. Epicier, Phys. Rev. B **48**, 10583 (1993).

[23] K. M. Freedy, P. M. Litwin, and S. J. McDonnell, ECS Trans. **77**, 11 (2017).

[24] See Supplemental Material at http://link.aps.org/supplemental/10.1103/PhysRevMaterials.3.104001 for a description of our two-color implementation of TDTR, a sensitivity analysis of relevant parameters in the Au/MoS_2 system, and further discussion of the specific series resistance model implemented, all XPS spectra, details of oxide composition analysis, and layer thickness calculation.

[25] J. Liu, G.-M. Choi, and D. G. Cahill, J. Appl. Phys. **116**, 233107 (2014).

[26] P. Jiang, X. Qian, X. Gu, and R. Yang, Adv. Mater. **29**, 1701068 (2017).

[27] S. Sahoo, A. P. S. Gaur, M. Ahmadi, M. J. F. Guinel, and R. S. Katiyar, J. Phys. Chem. C **117**, 9042 (2013).

[28] R. Yan, J. R. Simpson, S. Bertolazzi, J. Brivio, M. Watson, X. Wu, A. Kis, T. Luo, A. R. Hight Walker, and H. G. Xing, ACS Nano **8**, 986 (2014).
[29] M. Goni, J. Yang, and A. J. Schmidt, Nano Res. **11**, 2173 (2018).
[30] L.-B. Xiong, J.-L. Li, B. Yang, and Y. Yu, J. Nanomater. **2012**, 831524 (2012).
[31] M. J. Jackman, A. G. Thomas, and C. Muryn, J. Phys. Chem. C **119**, 13682 (2015).
[32] M. Jeong, J. P. Freedman, H. J. Liang, C.-M. Chow, V. M. Sokalski, J. A. Bain, and J. A. Malen, Phys. Rev. Appl. **5**, 014009 (2016).
[33] A. Rafati, R. Ter Veen, and D. G. Castner, Surf. Interface Anal. **45**, 1737 (2013).
[34] C. M. Smyth, R. Addou, S. McDonnell, C. L. Hinkle, and R. M. Wallace, 2D Mater. **4**, 025084 (2017).
[35] B. C. Gundrum, D. G. Cahill, and R. S. Averback, Phys. Rev. B **72**, 245426 (2005).
[36] A. Giri, J. T. Gaskins, B. F. Donovan, C. Szwejkowski, R. J. Warzoha, M. A. Rodriguez, J. Ihlefeld, and P. E. Hopkins, J. Appl. Phys. **117**, 105105 (2015).
[37] R. Cheaito, K. Hattar, J. T. Gaskins, A. K. Yadav, J. C. Duda, T. E. Beechem, J. F. Ihlefeld, E. S. Piekos, J. K. Baldwin, and A. Misra, Appl. Phys. Lett. **106**, 093114 (2015).
[38] R. B. Wilson and D. G. Cahill, Phys. Rev. Lett. **108**, 255901 (2012).
[39] B. M. Foley, S. C. Hernández, J. C. Duda, J. T. Robinson, S. G. Walton, and P. E. Hopkins, Nano Lett. **15**, 4876 (2015).
[40] K. M. Freedy, M. G. Sales, P. M. Litwin, S. Krylyuk, P. Mohapatra, A. Ismach, A. V. Davydov, and S. J. McDonnell, Appl. Surf. Sci. **478**, 183 (2019).
[41] T. C. Tisone and J. Drobek, J. Vac. Sci. Technol. **9**, 271 (1972).
[42] N. Tsud, F. Šutara, I. Matolínová, K. Veltruská, V. Dudr, V. Cháb, K. C. Prince, and V. Matolín, Appl. Surf. Sci. **252**, 5428 (2006).
[43] N. Tsud, F. Šutara, I. Matolínová, K. Veltruská, V. Dudr, K. C. Prince, and V. Matolín, J. Phys.: Condens. Matter **22**, 265002 (2010).
[44] A. Bzowski and T. K. Sham, J. Vac. Sci. Technol. A **11**, 2153 (1993).
[45] Y. Terada, K. Ohkubo, T. Mohri, and T. Suzuki, Mater. Trans. **43**, 3167 (2002).
[46] S. Ahmad and S. Mukherjee, Graphene **3**, 52 (2014).
[47] D. Liu, Y. Guo, L. Fang, and J. Robertson, Appl. Phys. Lett. **103**, 183113 (2013).
[48] H. Zhong, R. Quhe, Y. Wang, Z. Ni, M. Ye, Z. Song, Y. Pan, J. Yang, L. Yang, and M. Lei, Sci. Rep. **6**, 21786 (2016).
[49] Y. Li, C. Cai, Y. Gu, W. Cheng, W. Xiong, and C. Zhao, Appl. Surf. Sci. **414**, 34 (2017).